

1 Design and analysis of an aluminum F-shape 2 bridge railing

doi:10.1533/ijcr.2004.0295

3 M H Ray and E Oldani

4 Worcester Polytechnic Institute, 100 Institute Road, Worcester, MA 01609

5 **Abstract:** This report describes the design and analysis of an extruded aluminum truss-work bridge
6 railing for NCHRP Report 350 test levels three and four conditions. The objective of this research is
7 to determine if the barrier will pass the NCHRP Report 350 full-scale crash tests for test levels three
8 and four by using the nonlinear dynamic finite element program LS-DYNA. A subsequent AASHTO
9 LRFD analysis supported the LS-DYNA results. The design documented in this report was found
10 to be of comparable strength to other F-shaped bridge railings so that successful crash test results are
11 highly likely.

12 **Key words:** Roadside safety, crashworthiness, highway safety, bridge railings, aluminum, crash testing,
13 design.

14 INTRODUCTION

15 There is a long history of successful crash test performance
16 with a variety of F-shape railings made using reinforced
17 concrete [1, 2]. The barrier discussed in this report uses
18 the same F-shape profile that has been successfully tested
19 before in the referenced research projects. Reinforced
20 concrete barriers attached to a bridge deck behave
21 essentially as rigid barriers so the primary issue to be
22 considered is, are ultimate strengths of the F-shape parapet
23 bridge railing and the F-shape aluminum median barrier
24 equal to or greater than the reinforced concrete or steel
25 variations of the barrier. If the aluminum F-shape bridge
26 railing is shown to be at least as strong as the tested
27 reinforced concrete barrier systems, it can be inferred
28 that the aluminum bridge railings would likewise result
29 in good crash test performance. In essence, prior crash
30 testing has demonstrated that a rigid F-shape barrier results
31 in acceptable test level four performance therefore any F-
32 shape barrier will result in similar crash test results as
33 long as the structural response is essentially rigid (i.e.,
34 there are no major deformations). With this in mind, the
35 objective of this project was to compare the strength of
36 the F-shape aluminum parapet bridge railing to the known

crash test performance of other F-shape barriers to 37
determine if the aluminum barrier is at least as strong as 38
the reinforced concrete F-shaped barriers. Additionally, 39
the likely performance of the aluminum F-shape barrier 40
was assessed in nonlinear dynamic finite element 41
simulations for the Report 350 Test 3-11 conditions (i.e., 42
the pickup truck test) to determine the likely result of a 43
full-scale crash test [3]. Following the dynamic analysis 44
for test level three, an LRFD analysis corresponding to 45
test level four was performed according to the procedure 46
outlined in section 13 of the AASHTO LRFD Bridge 47
Specification [4]. 48

Barrier Description 49

The aluminum parapet bridge railing, shown in Figure 1, 50
is an 856-mm high F-shape barrier made up of (1) a base 51
plate, (2) a post, (3) a lower truss-core extruded panel, (4) 52
an upper truss-core extruded panel, (5) a top cap, (6) 53
backing plates and (7) a variety of toe clips and other 54
fasteners. The various components are interlocked with 55
each other and secured using stainless steel cap screws. 56

The base plate, shown in Figure 2, provides a connection 57
between the bridge deck and the post and lower truss- 58
core panel of the bridge railing. The base plate is made 59
using 6061-T6 aluminum alloy and is fastened to the deck 60
using two one-inch diameter A325 galvanized steel bolts 61
in the front and two M16 bolts in the rear of each base 62
plate. The bolts are threaded into an epoxy insert in the 63
bridge deck. M24 bolts in the front resist the overturning 64
moment of the post whereas the M16 bolts in the rear 65
serve primarily an alignment purpose. The base plate is 66

Corresponding Author:

Tel Fax
Email:

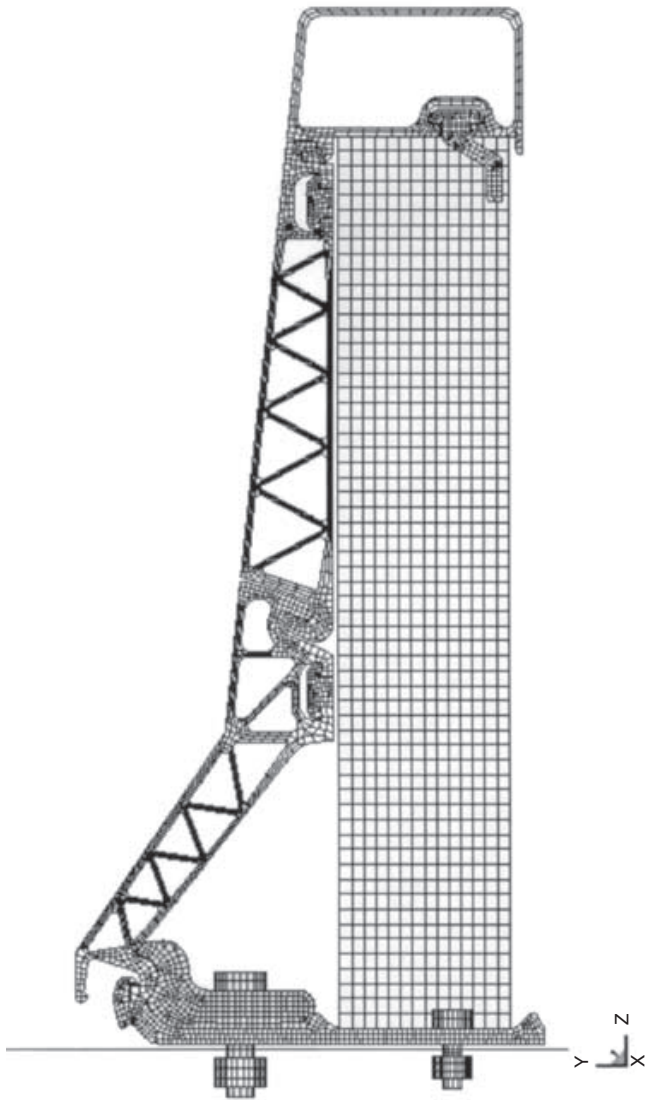


Figure 1 Finite element model of the aluminum parapet bridge railing.

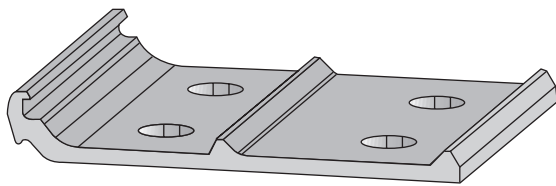
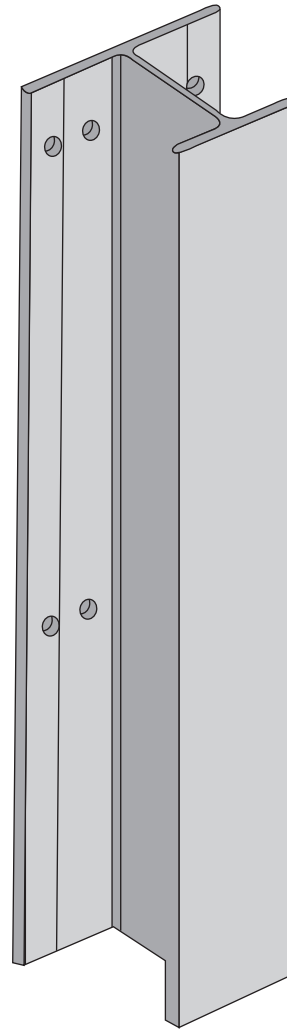


Figure 2 Three-dimensional model of the aluminum bridge parapet base plate.

67 welded to the post along the web of the post as described
68 below.

69 The post, shown in Figure 3, is extruded using 6061-
70 T6 aluminum alloy. The shape of the post was modified
71 during the project to ensure that the compression flange
72 (i.e., the rear flange) did not buckle in an impact. Figure
73 3 also shows the inertial properties and a cross-section
74 plot of the new post geometry. The web of the post is
75 welded to the base plate shown in Figure 2, which is in
76 turn bolted to the bridge deck using two M24 A325
77 structural steel bolts.



	Post version A	Post version B
Area [mm ²]	4007.22	5009.28
Perimeter [mm]	960.59	1028.88
Radii of giration x [mm ²]	44.84	50.01
Radii of giration y [mm ²]	79.13	90.18
Jx [mm ⁴]	8.02E+06	1.25E+07
Jy [mm ⁴]	1.67E+07	2.17E+07

Figure 3 Three-dimensional model, cross-section view and inertial properties of the aluminum bridge parapet post.

78 When the structure is loaded, the flexural moment is
79 transferred to the deck of the bridge through a triangular
80 truss composed of the lower truss-core panel, the base
81 plate and the back flange of the post (see Figure 1). The
82 aluminum post initially loads in bending but it is quickly
83 restrained by the triangular truss formed with the lower
84 panel. In particular, the lower panel loads in tension while

85 the post and the base plate are compressed. The upper
 86 part of the barrier (i.e., the upper truss-core panel shown
 87 in Figure 5) is loaded in bending as a whole system. The
 88 outer skin of the upper panel is loaded in tension while
 89 the rear flange of the post is in compression. The neutral
 90 axis of the system is located somewhere between the panel
 91 and the rear flange of the post, therefore, the front flange
 92 of the post is mainly loaded in shear, transferred through
 93 the upper clamp bar. Since the base of the posts is not
 94 significantly loaded in bending, only the web of the posts
 95 is welded to the base plate. Not welding the flanges avoids
 96 heat-affecting the base of the posts.

97 The top cap, shown in Figure 4, is extruded using 6063-
 98 T6 aluminum alloy. The top cap was modeled using a
 99 length of 6350 mm but it would generally be manufactured
 100 in lengths of 6 to 7 m. The top cap interlocks with the
 101 upper truss-core panel with an 18-8 stainless steel bolt
 102 and clamp bar and is secured to the top of the post with
 103 a steel cap screw. The structural function of the top rail
 104 is preventing the upper panel from bowing between the posts.
 105 It acts as a longitudinal beam, reacting to the longitudinal
 106 flexural moments that the external loads generate in the
 107 upper panel.

108 The upper truss-core panel, shown in Figure 5, is
 109 extruded using 6063-T6 aluminum alloy. The panel was
 110 modeled using a length of 6350 mm but it would generally
 111 be manufactured in the range of 6 to 7 m. The upper
 112 truss-core panel interlocks with the shape of the lower
 113 truss-core panel and the ridge top. The upper clamp bar
 114 fastens the upper edge of the upper truss-core panel to
 115 the post and backing plate using two 18-8 stainless steel
 116 bolts.

117 The lower truss-core panel, shown in Figure 6, is
 118 extruded using 6063-T6 aluminum alloy. The panel was
 119 also modeled using a length of 6350 mm but it would
 120 generally be manufactured in lengths of 6 to 7 m. The
 121 lower panel interlocks with the shape of the base plate on
 122 the lower edge and the upper truss-core panel on the
 123 upper edge. The lower clamp bar fastens the upper edge
 124 of the lower truss-core panel to the post using four 18-8
 125 stainless steel bolts. The lower clamp bar attaches the
 126 lower truss-core panel to the backing plate at mid-span
 127 locations using only two stainless steel bolts.

128 The backing plates are located at midspan between two
 129 posts. Shorter base plates combined with standard toe
 130 clips are also positioned at the same locations. First the

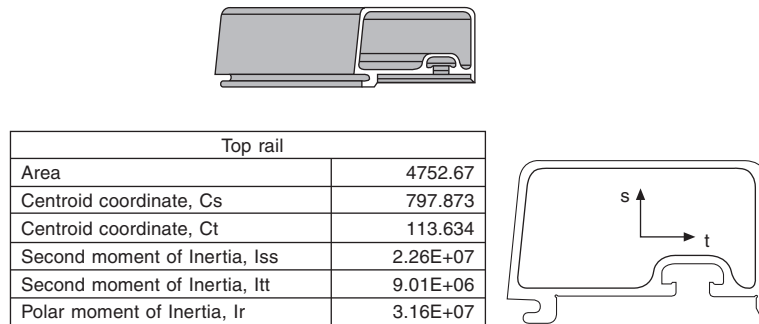


Figure 4 Three-dimensional model, cross-section view and inertial properties of the aluminum bridge parapet top rail.

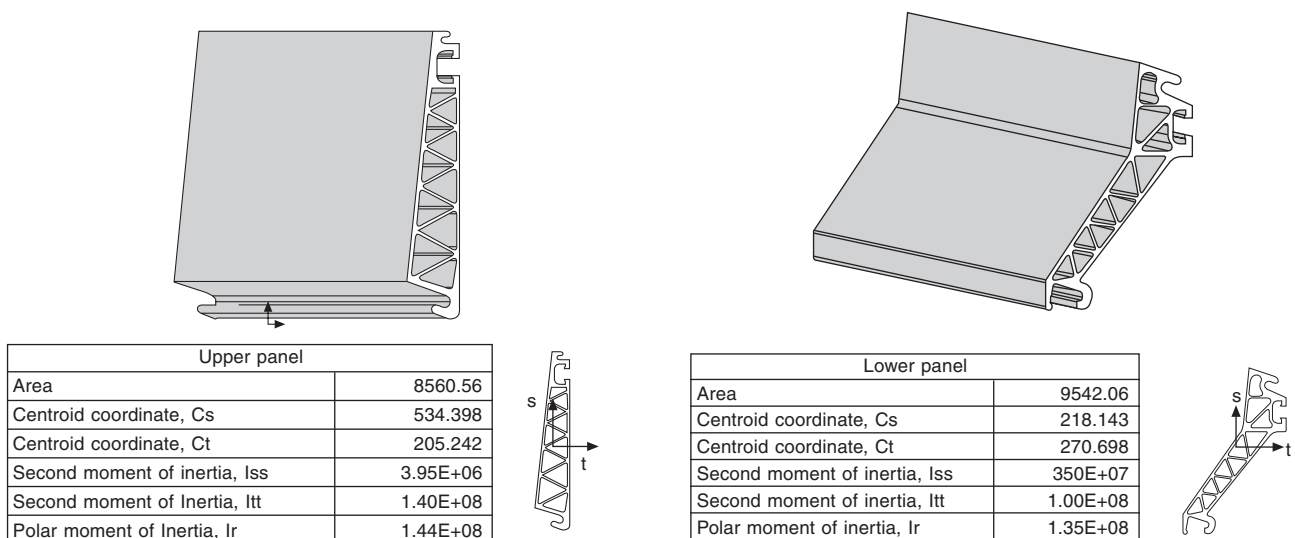


Figure 5 Three-dimensional model, cross-section view and inertial properties of the upper truss-core panel of the aluminum bridge parapet.

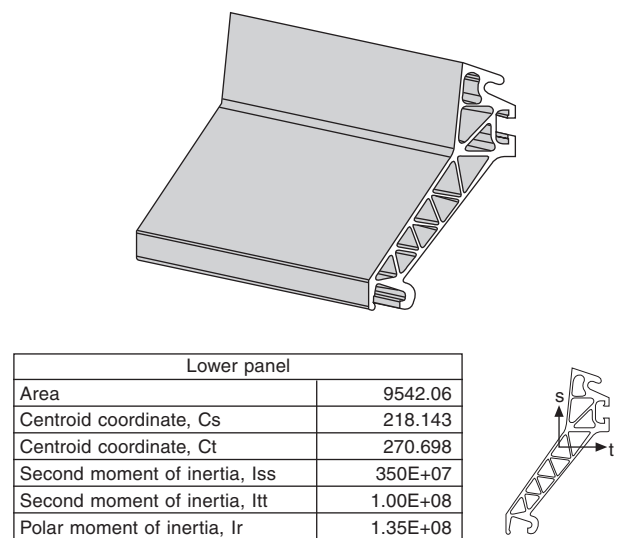


Figure 6 Three-dimensional model, cross-section view and inertial properties of the lower truss-core panel of the aluminum bridge parapet.

131 base plates are installed on the deck of the bridge, followed
 132 by toe clips and posts, then a series of top rails are fixed
 133 to the posts. The top rail serves as a hanger to position a
 134 series of upper panels that are attached to the posts with
 135 clamp bars. The bottom panel is then positioned on the
 136 post bases and the bottom of the toe clips, rotated into
 137 place and interlocked with the upper panels.

138 DYNAMIC ANALYSIS FOR TEST LEVEL THREE

139 Background

140 In general, the U.S. Federal Highway Administration
 141 (FHWA) has required that bridge railings be evaluated in
 142 full-scale crash tests since 1986. A memorandum from
 143 the FHWA dated 16 May 2000 outlines a procedure for
 144 analyzing untested bridge rail configurations that are similar
 145 to tested systems [5]. The procedure was developed by
 146 the State of Colorado and is outlined in a 21 July 1998
 147 document that is attached to the FHWA memorandum.
 148 Basically, the procedure involves the following syllogism:
 149 if a particular untested bridge railing can be shown to
 150 have the same ultimate strength as a geometrically similar
 151 bridge railing that has passed the Report 350 full-scale
 152 crash tests, then it can be inferred that the untested railing
 153 would also have passed the Report 350 full-scale crash
 154 tests. Stated more explicitly for the case of a rigid concrete
 155 barrier, the syllogism is:

- 156 • If a bridge railing:
 - 157 – Remains rigidly connected to the bridge deck during
 - 158 and after an impact and
 - 159 – The barrier structure is essentially undamaged,
- 160 • Then the bridge railing can be considered rigid.
- 161 • And if two bridge railings have the same shape and are
- 162 essentially rigid,
- 163 • Then they should experience similar impact
- 164 performance in the corresponding Report 350 tests.

165 This procedure was used to (1) determine the loads on
 166 a rigid F-shape concrete bridge railing usually considered
 167 to satisfy Report 350 test level four and (2) apply those
 168 same loads to an aluminum F-shape bridge railing to
 169 determine if the aluminum barrier responds in an
 170 essentially rigid manner. If the F-shape barrier does not
 171 experience excessive deformations under the loadings
 172 observed in a rigid F-shape barrier test, the response of
 173 the vehicle and its occupant can be assumed to be identical.
 174 Since the rigid concrete F-shape barrier passed the test
 175 level three and four criteria it can therefore be assumed
 176 that the aluminum F-shape barrier would likewise pass.

177 A dynamic analysis of the aluminum parapet and median
 178 barriers was performed using the finite element program
 179 LS-DYNA. The purpose of the analysis was to predict
 180 the performance of the two aluminum barrier systems in
 181 Report 350 Test 3-11 crash tests (i.e., the 2000 kg pickup
 182 truck striking the barrier at 100 km/hr and 25 degrees).
 183 A detailed finite element model of the barrier was developed
 184 and an already-developed finite element model of a 2000

kg pickup truck was used for this analysis. The analysis
 was performed using the program LS-DYNA.

Loads on F-shape barriers in Test 3-11

While a reinforced concrete F-shape bridge railing rigidly
 cast into the bridge deck is considered a test-level three
 barrier, no tests could be found in the roadside safety
 literature that exactly match Test 3-11 (i.e., a 2000 kg
 full-size pickup truck striking the barrier at a 25 degree
 angle at 100 km/hr). The reason for this is that most
 bridge rail testing was performed prior to the publication
 of NCHRP Report 350 according to the AASHTO bridge
 railing testing procedure.

An 810 mm tall reinforced concrete F-shape bridge
 railing was tested using the old AASHTO Bridge
 Specification criteria at Texas Transportation Institute
 (TTI) and the results are reported in both a TRB paper
 and an FHWA report [6, 1]. The AASHTO Bridge
 Specification PL-2 pickup truck test is similar to NCHRP
 Report 350 Test 3-11 except a 20 rather than 25 degree
 impact angle is used and the truck weight is 5,400 lbs
 rather than 4,500 lbs. The 810 mm tall F-shape, however,
 is considered to satisfy the Report 350 requirements since
 it also passes the higher level AASHTO PL-3 test criteria.
 If it can be demonstrated that the aluminum F-shape
 barriers can provide the same ultimate strength as the
 tested reinforced concrete F-shape barrier, then this should
 form a basis for FHWA acceptance according to the 16
 May 2000 FHWA Memorandum.

Estimating the loads experienced by a rigid F-shape
 barrier under Test 3-11 conditions, therefore, is a little
 more complicated than it would be if there were a full-
 scale test of a reinforced concrete F-shape bridge railing
 available. Since there is no such test available, a finite
 element analysis of the AASHTO PL-2 test was performed
 to compare the results with the crash test. The F-shape
 was modeled by using a surface of rigid (i.e., non-
 deformable) shells in the geometry of the F-shape barrier.
 A C2500 pickup truck model with fully functioning
 suspension, steering and tire models was used as the vehicle
 model [7, 8]. The vehicle was set up initially for Report
 350 testing so its mass was 2000 kg corresponding to the
 Report 350 test conditions. Additional mass was added to
 the model to ballast the model up to 2408 kg, as close to
 the 2450 kg AASHTO specifications as could be achieved
 while also balancing the rotatory moments of inertia.

The finite element simulation was then run at exactly
 the same speed and angle as the TTI test. The results are
 summarized in Table 1 and in Figures 7 and 8. As shown
 in the sequential photographs in Figures 7 and 8, the
 overall qualitative response of the vehicle in the finite
 element simulation was very similar to the actual full-
 scale crash test. Figure 7 shows a downstream view of the
 crash event and Figure 8 shows an overhead view of the
 event. Table 1 shows the quantitative parameters calculated
 by the TRAP program to evaluate full-scale crash tests.
 As shown in Table 1, the finite element simulation

Table 1 Comparison of TTI Test 7069-4 and the finite element simulation of PL-2 test conditions

Test parameter	Test 7069-4	Simulation
Test vehicle		
Type	81 Chevrolet PU	C2500
Mass	2470 kg	2408 kg
Impact conditions		
Velocity	105.2 km/h	105.2 km/hr
Angle	20.4 deg	20.4 deg
Exit conditions		
Velocity	91.6 km/hr	86.6 km/hr
Angle	7.4 deg	8.0 deg
Vehicle accelerations (50 msec averages)		
Longitudinal	4.7 g's	8.2 g's
Lateral	13.1 g's	13.9 g's
Occupant impact velocity (OIV)		
Longitudinal	3.8 m/s	5.1 m/s
Lateral	7.3 m/s	7.4 m/s
Occupant ridedown acceleration (ORA)		
Longitudinal	1.2 g's	5.1 g's
Lateral	5.9 g's	15.2 g's

241 redirected the vehicle at almost the same exit angle but
 242 the vehicle was traveling 5 km/hr slower when it lost
 243 contact in the simulation than in the full-scale test. This
 244 is also reflected in the other parameters where the vehicle
 245 50 msec average, occupant impact velocity and occupant
 246 ridedown velocity are all a little higher in the simulation
 247 for the longitudinal direction than in the full-scale test.
 248 This is a result of the barrier-vehicle friction being higher
 249 in the simulation than in the test. It would be possible to
 250 adjust the friction coefficients such that exactly the same
 251 values were obtained but the simulation values shown are
 252 more conservative (i.e., they estimate higher than actual
 253 loadings) so it was decided to keep the usual values. The
 254 values for the vehicle 50 msec average acceleration and
 255 occupant impact velocity in the lateral direction were nearly
 256 identical between the test and simulation indicating that
 257 the lateral loading is accurately represented by the finite
 258 element model. The lateral occupant ridedown acceleration
 259 was much higher in the simulation. This corresponded to
 260 a very high "tail slap" event in the simulation when the
 261 rear of the vehicle struck the barrier. Since the finite
 262 element simulation over-predicts the responses, the
 263 simulation yields conservative estimates of the barrier
 264 loading which is desirable from a design perspective. Next,
 265 a finite element simulation of the Test 3-11 was performed.
 266 Since the finite element model conservatively predicted
 267 the results of the AASHTO PL-2, we can be reasonably
 268 confident that the model will likewise conservatively predict
 269 the results of an actual crash test of a rigid concrete F-
 270 shape were performed. The same C2500 truck and rigid
 271 F-shape barrier models were used to perform a finite
 272 element simulation corresponding to Report 350 Test 3-
 273 11. This simply involved changing the impact conditions
 274 from the previous AASHTO PL-2 simulation to conform
 275 to the Test 3-11 conditions. The results of this simulation

are summarized in Table 2 and Figure 9. Not surprisingly, the finite element simulation predicts that the rigid F-shape barrier would pass the Report 350 test criteria. The quantitative values for the simulation are shown in Table 2 and sequential views of the impact are shown in Figure 9.

In principle, the finite element model of the C2500 pickup truck could be used to simulate an impact using a detailed model of the aluminum parapet and median railings. Unfortunately, the truss-core structure of the aluminum railings makes this impractical because the element size required to capture all the detail of the truss work is very small resulting in a very large model. Instead, the rigid F-shape barrier model discussed in the previous paragraphs was used to capture a time history of the loads at each node on the face of the barrier. This time history was saved in a separate file and then used to apply the same loadings to a very detailed model of each of the aluminum barriers. A much more detailed and complete description of the finite element models and the methods for collecting the load data for this problem can be found in a thesis by Oldani but the procedure is summarized below [9].

A layer of shell elements was placed across the face of the barrier to serve as a sensing surface for the loads. These elements were made of null material so they had no stiffness or mass and therefore did not affect the response of either the vehicle or the barrier. The sensing elements were rigidly connected to the barrier and a contact definition was placed on the surface such that the force transmitted by the vehicle to the barrier could be measured at each time step. The sensing surface was 5 m long and included the whole region of the barrier where contact was expected based on past crash testing. The sensing elements were approximately 50 mm square so the load was recorded at 3,434 specific locations on the face of the barrier (i.e., 101 rows in the longitudinal direction and 34 in the vertical direction along the face of the barrier). The resultant load at each of these locations was calculated and saved in an external file at 6.6 : s (i.e., $6.6(10)^{-3}$ msec) intervals such that when the run was complete, a time history file of the loads at each of these locations was obtained.

Figure 10 shows plots of the lateral (i.e., normal), longitudinal (i.e., tangent) and vertical load time histories resulting from a Test 3-11 impact with a rigid F-shape barrier. As shown in Figure 10, there are two distinct signal signatures; the first shows the primary impact with the vehicle that starts at the time of impact and ends at roughly 120 msec. The second signature corresponds to the back of the pickup truck "slapping" the barrier. This event occurs roughly between 180 and 250 msec. The maximum lateral load observed in the finite element simulation of Test 3-11 during the primary impact event (i.e., up until 120 msec after impact) was 410 kN (i.e., 92 kips) and the average in this range was approximately 300 kN (i.e., 67 kips). The maximum longitudinal and vertical

333 loads during this phase of the collision were both less
 334 than 125 kN (i.e., 28 kips) as shown in Figure 10. Figure
 335 11 shows the average heights of the lateral, longitudinal
 336 and vertical load resultants above the bridge deck. The
 337 average height of the lateral load resultant during the first
 338 and phase of the collision was 545 mm and the maximum
 339 height was 695 mm, well below the 856 mm (i.e., 33.7 in)
 340 height of the barrier.

341 Interestingly, the AASHTO LRFD Bridge Specification
 342 equivalent static loads for Test Level 3 require the use of
 343 a 240 kN lateral load applied 685 mm above the bridge

344 deck. The AASHTO equivalent static loads are similar to
 345 the values found in the dynamic finite element simulation
 346 of the Test Level 3 event; the dynamic load is a little
 347 higher but applied at a slightly lower level. This indicates
 348 that the AASHTO LRFD procedure for test level three
 349 should result in reasonably similar designs to this dynamic
 350 analysis.

351 The second signature in Figures 10 and 11 indicates
 352 the impact between the bed of the truck and the barrier.
 353 The bed “slapping” the bridge railing toward the end of
 354 the event is a shorter duration, lower magnitude impact

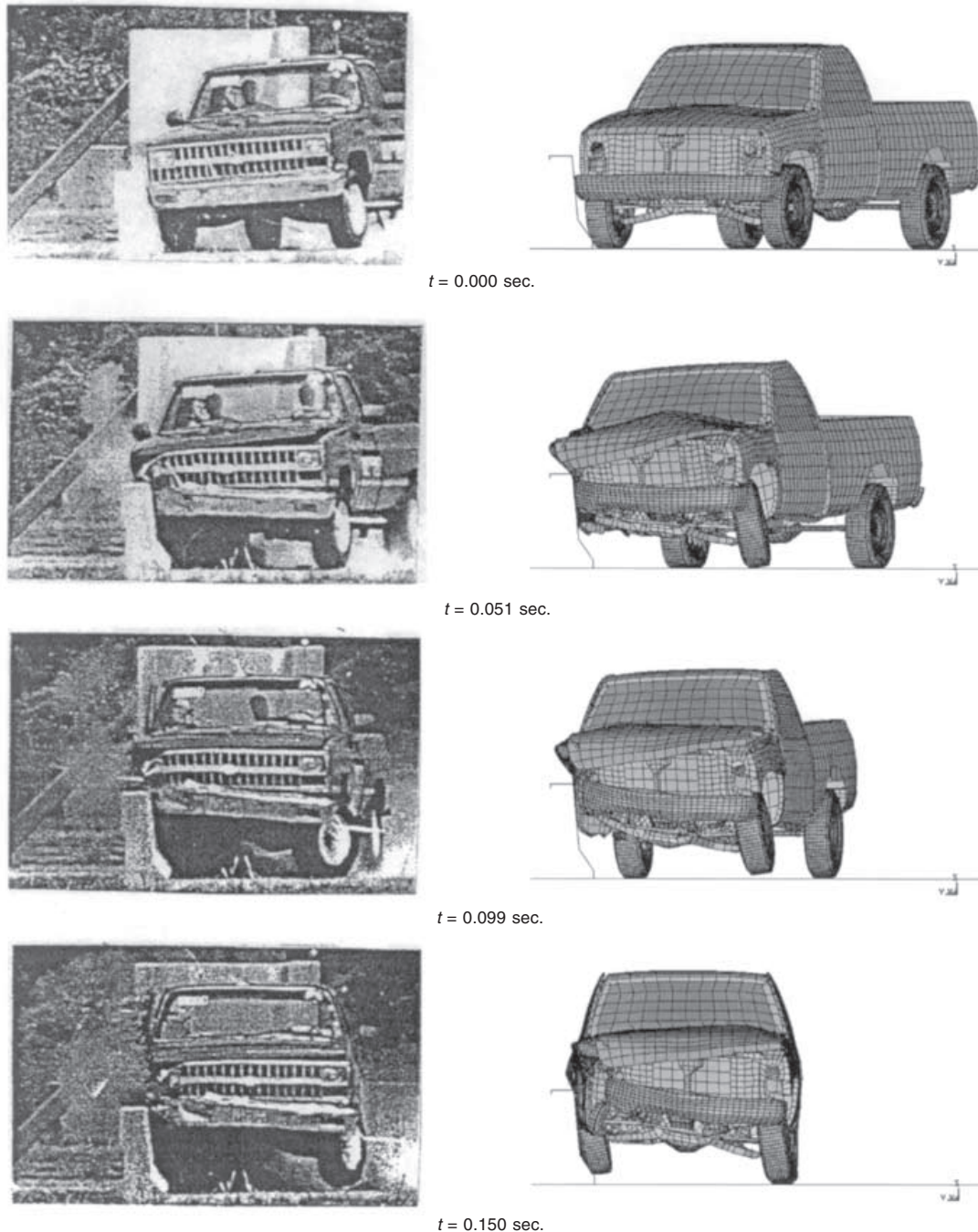


Figure 7 Downstream view comparison of AASHTO PL-2 full-scale crash and a finite element simulation of an impact with a rigid F-shaped bridge railing.

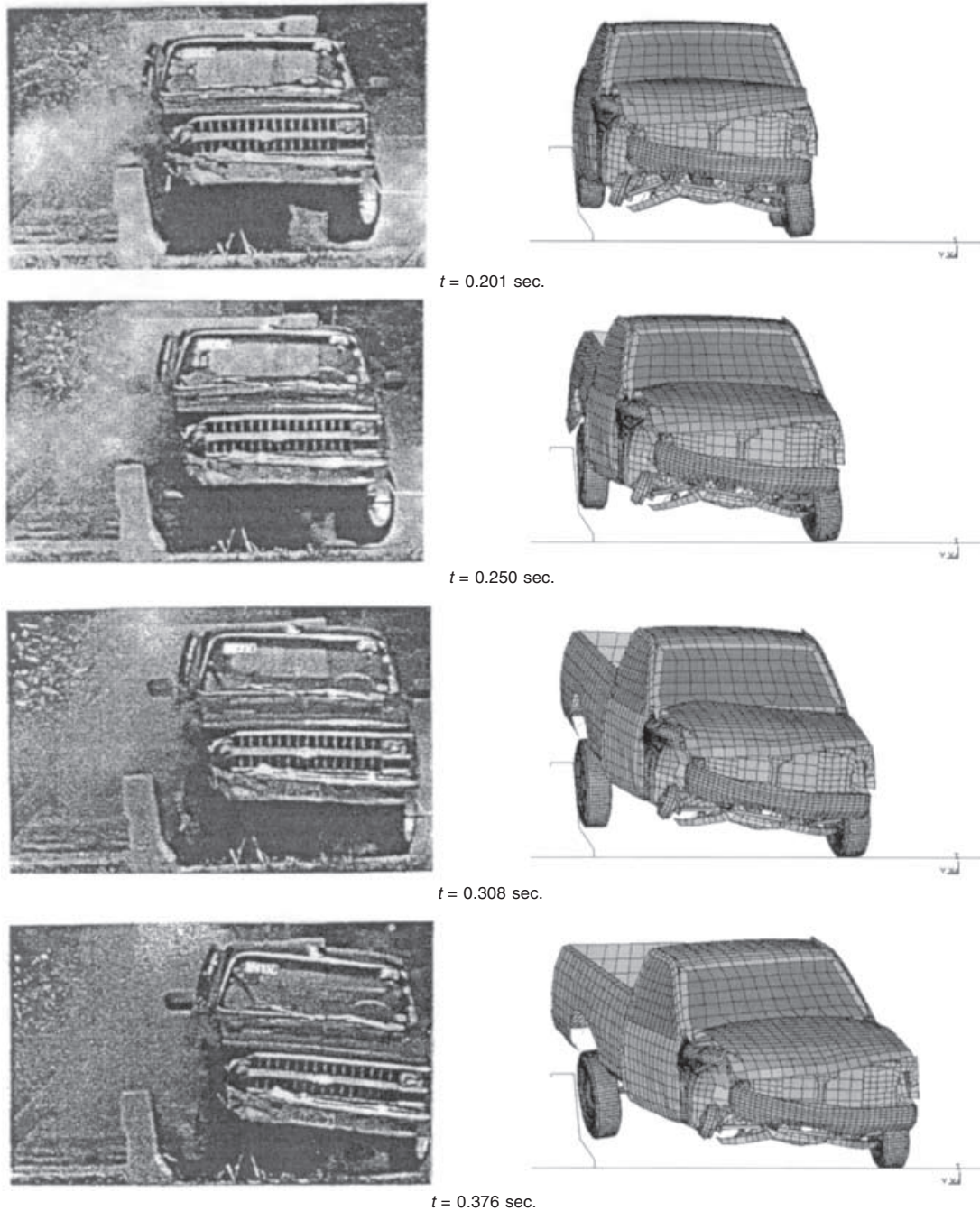


Figure 7 (Continued)

355 event. The maximum lateral loading in this second phase
 356 of the collision is 213 kN (i.e., 48 kips) and the average is
 357 about 125 kN (i.e., 28 kips). The maximum height of
 358 lateral load application in the second phase of the collision
 359 is 785 mm but the average is a much lower 391 mm as
 360 shown in Figure 11.

361 Once the load at every node on the barrier face was
 362 known for every time step during the Test 3-11 impact
 363 with the rigid F-shape barrier, this time-based load was
 364 applied to the face of the aluminum barriers of interest in
 365 this project.

**Application of dynamic loads to the F-shape parapet
 bridge railing**

**366
 367**

368 As discussed in the previous section, a time history file of
 369 the loads at 3,434 specific points on the barrier was obtained
 370 by performing a finite element analysis of a Report 350
 371 Test 3-11 of a rigid F-shape bridge railing. These loads
 372 were then applied to the finite element model of the
 373 aluminum bridge railing and the aluminum median barrier
 374 described at the beginning of this paper. Applying this
 375 file of loads as a function of position and time to the
 376 prospective aluminum barriers is equivalent to performing

376

377 a finite element simulation or full-scale test of the barrier.
 378 The result of such an analysis is the stresses and strains
 379 experienced by the two aluminum barrier configurations
 380 under Test 3-11 conditions. If the barriers withstand the
 381 application of the forces with acceptable stresses and only
 382 small localized permanent deflections, the barriers can be
 383 judged to satisfy the test level three conditions.

384 A detailed finite element model of the aluminum F-
 385 shape bridge parapet railing, shown earlier in Figures 2
 386 and 8, was developed. Because the truss work in the panels
 387 is very thin, a very detailed model containing over 600,000
 388 elements (579,950 of which were solid elements used to
 389 represent the intricate extruded aluminum truss core panels

and top rails) with very small elements was necessary. A
 390 0.5 : s time step was required due to the small element
 391 size and the total simulation time was 317 msec. A much
 392 more detailed and complete description of the finite element
 393 models and the methods for collecting the load data for
 394 this problem can be found in a thesis by Oldani [9].
 395

The results of the application of the Test 3-11 loads are
 396 summarized in Figure 12. There were only local plastic
 397 deformations of the post near the front edge of the weld.
 398 These localized stresses, shown as red spots in Figure 12,
 399 were above the yield stress for 6061-T6 aluminum but
 400 still well below the failure limit. The maximum loading
 401 occurred at the first post downstream of the impact at
 402

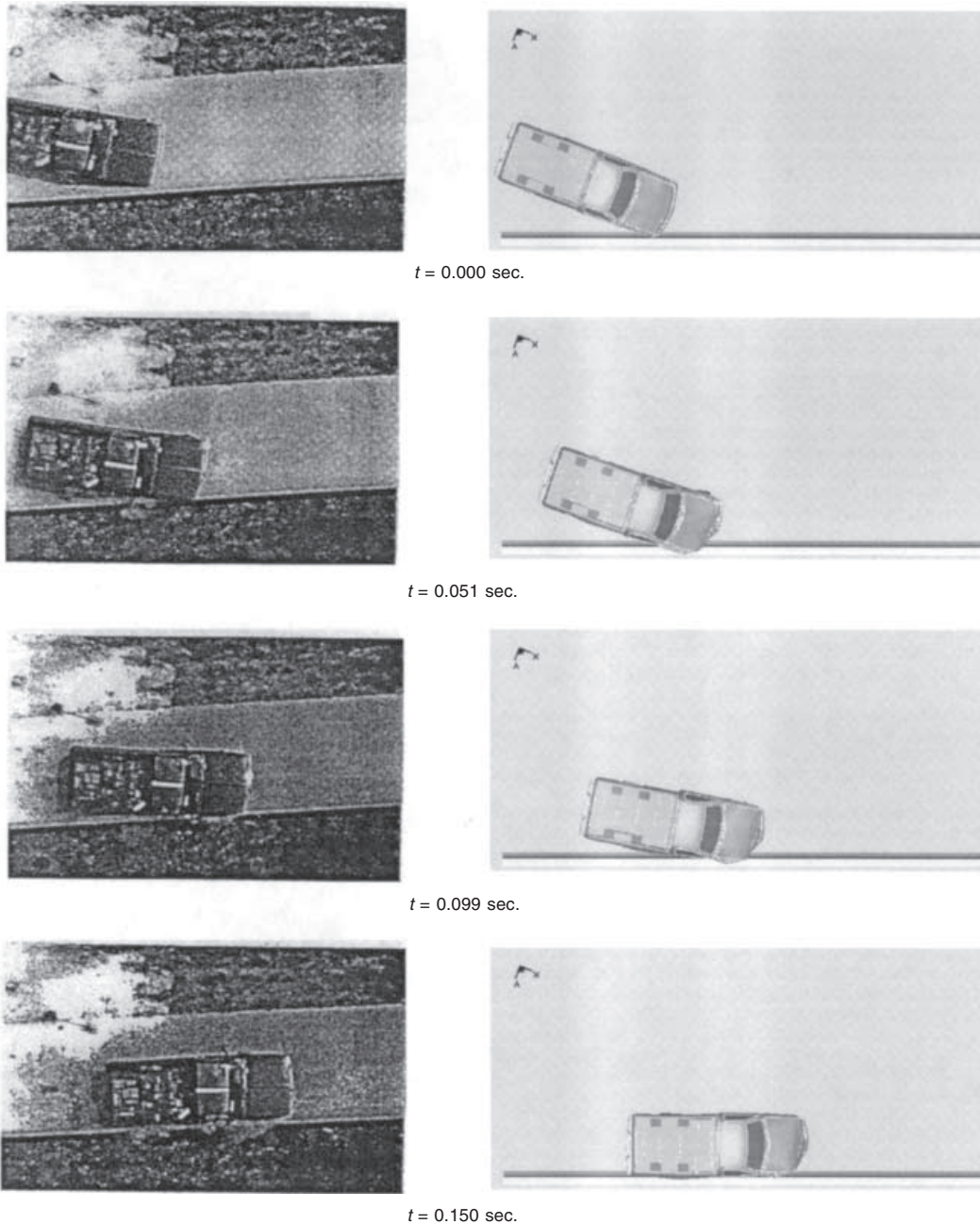


Figure 8 Overhead comparison of AASHTO PL-2 full-scale crash and a finite element simulation of an impact with a rigid F-shaped bridge railing.

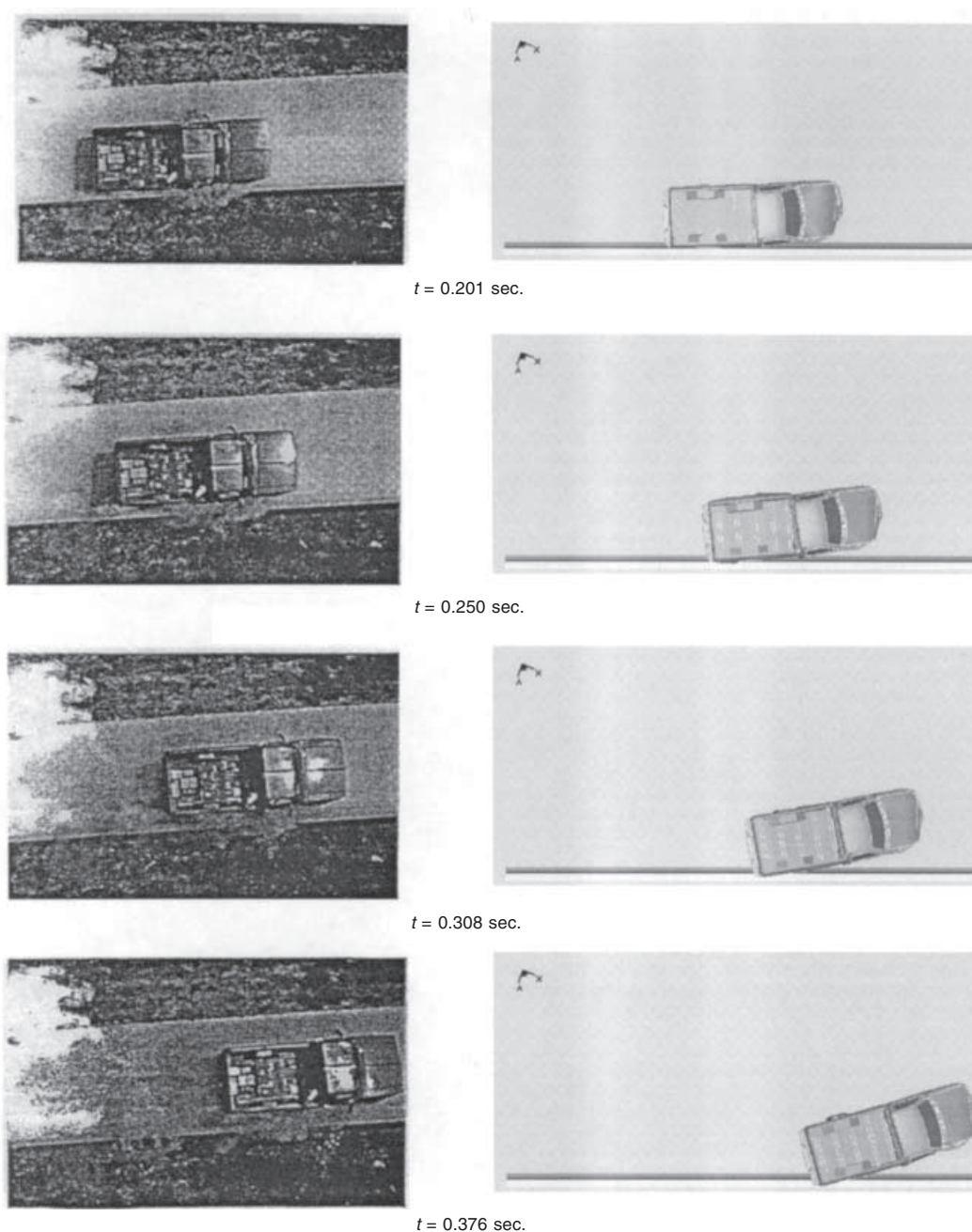


Figure 8 (Continued)

403 about 60 msec after the impact. The compression flange
 404 of the post, a region where the analysis had uncovered
 405 buckling problems with earlier versions of the post,
 406 experienced stress well under the yield stress at the
 407 maximum post loading. There were also some localized
 408 permanent deformations of the face of the truss-core panels
 409 where the front bumper and wheel rims contacted the
 410 barrier. All of the interlocked connections remained intact
 411 and showed no tendency to pull apart during the impact.

412 Likewise the bolted connections and clamp bars remained
 413 in the elastic region even at the time of maximum loading.
 414 The global lateral deflections of the barrier measured
 415 at several points at the very top of the bridge railing were
 416 obtained. The maximum dynamic lateral loading occurred

417 roughly at the midspan and was a modest 37 mm. There
 418 was a significant spring-back effect such that the final
 419 maximum permanent deflection at the top of the barrier
 420 was only 5 mm. The reason for this is that there is very
 421 little plastic deformation anywhere in the barrier so most
 422 of the strain energy is returned elastically after the
 423 maximum loading has passed.

424 The upper truss-core panel absorbs about 30 percent
 425 of the strain energy and the top rail absorbs about 15
 426 percent of the strain energy at the peak loading. The lower
 427 truss-core panel, the post web, the post flanges and the
 428 toe clips are responsible for the remaining strain energy
 429 absorption in roughly equal amounts. About 65 percent
 430 of the total strain energy remains elastic explaining the

431 very small lateral deflections. The remaining 35 percent
 432 of total strain energy is accounted for by a variety of
 433 localized deformations in the face of the barrier and the
 434 base of the post as described earlier.

435 Since only minor localized deformations occurred and
 436 the barrier retained its structural integrity throughout
 437 the impact event, the aluminum parapet bridge railing is
 438 essentially rigid. A maximum dynamic deflection of 37
 439 mm and a permanent lateral deflection of 5 mm is very
 440 small considering the geometry of the railing and the
 441 severity of the impact. Since the aluminum parapet bridge
 442 railing performs as an essentially rigid barrier, it can be
 443 presumed that a full-scale crash test of this barrier would
 444 result in essentially the same responses as a full-scale test

445 with a concrete barrier rigidly attached to the bridge deck.
 446 Since a concrete F-shape barrier is already presumed to
 447 satisfy the test level three criteria it can be inferred that
 448 the aluminum parapet bridge railing also satisfies Report
 449 350 test level three.

STATIC LRFD ANALYSIS FOR TEST LEVELS THREE AND FOUR 450
 451

Background 452

453 In principle a dynamic finite element simulation of a test
 454 level four impact between the two aluminum barriers could
 455 also be performed using exactly the same models discussed
 456 in the previous section. The 8000S vehicle available from

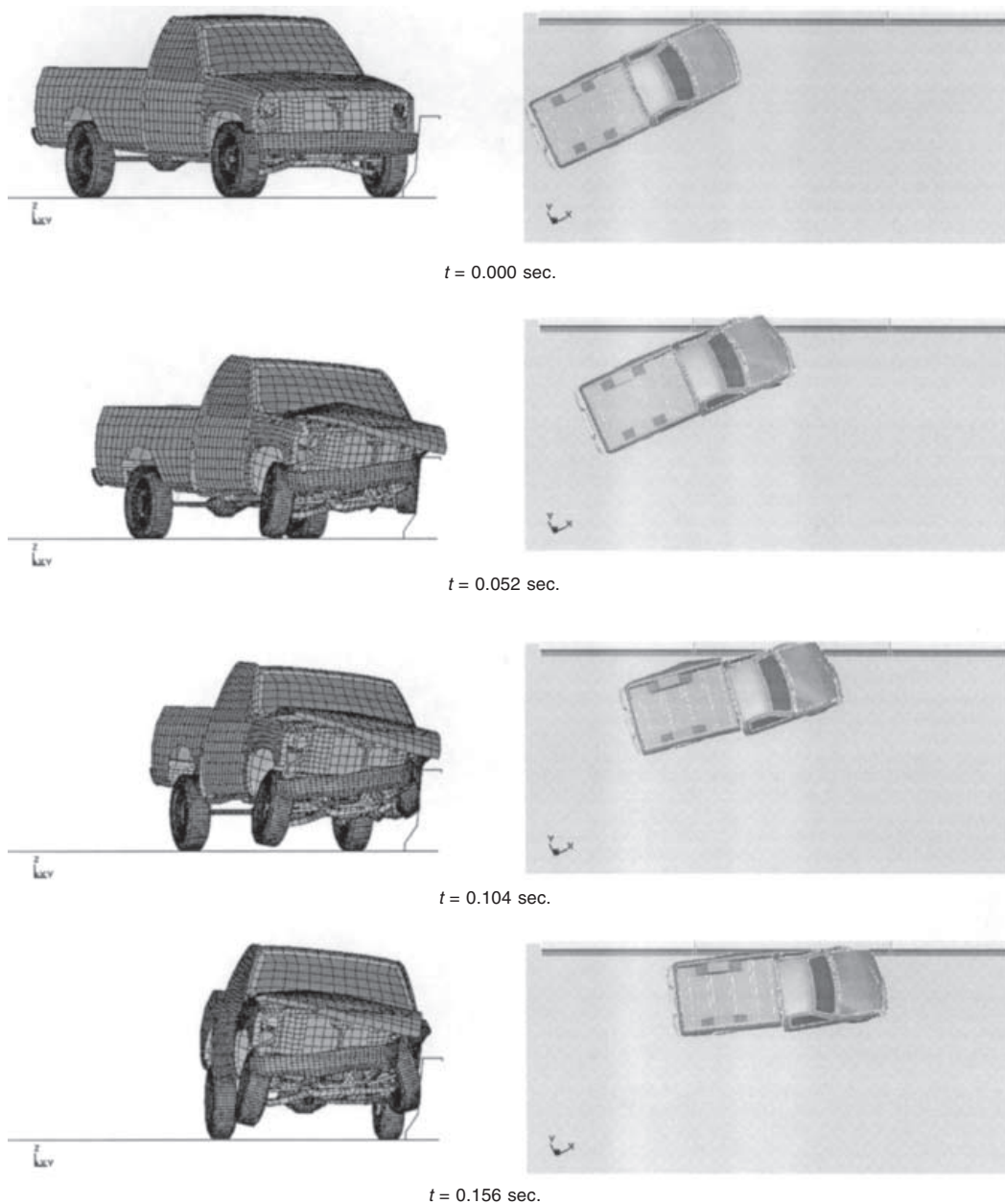


Figure 9 Sequential downstream and overhead views of a finite element simulation of an impact with a rigid F-shape bridge railing under Report 350 Test 3-11 conditions.

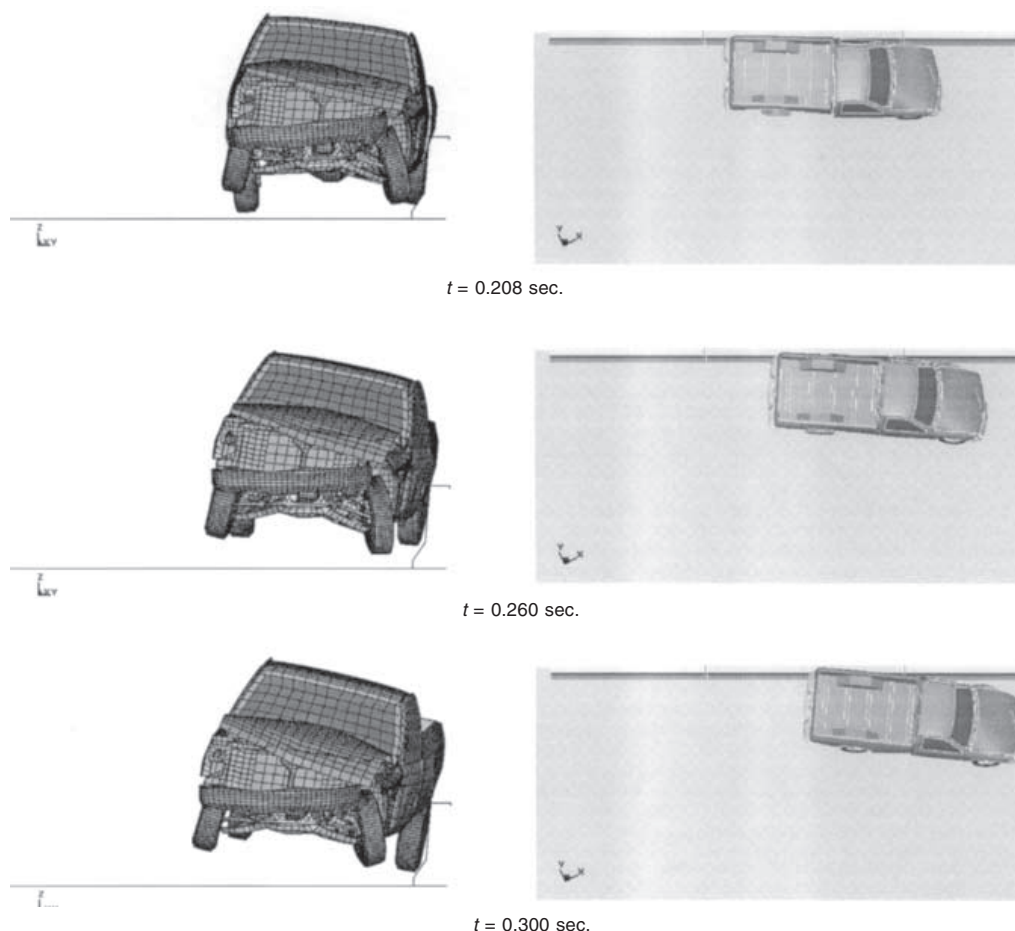


Figure 9 (Continued)

457 the National Crash Analysis Center is still in the
 458 development phase. Battelle and Oak Ridge National
 459 Laboratory (ORNL) were recently contracted to assess
 460 the fidelity of the model for use in NCHRP Report 350
 461 Test Level 4 impact simulations. Simulations of various
 462 full-scale tests of test level four impacts into rigid barriers
 463 were conducted independently by the two organizations.
 464 Their analyses identified several areas of concern in the
 465 model that were leading to erroneous results. Battelle,
 466 ORNL and the NCAC are currently in the process of
 467 enhancing the model for use in test level four impact
 468 simulations.

469 As an alternative, the AASHTO LRFD analysis
 470 procedure was used to evaluate the aluminum bridge railing
 471 design for test level four. If a rigid barrier (i.e., bridge
 472 railing) with the same basic shape as the untested barrier
 473 has been tested, all that must be done is to demonstrate
 474 that the untested barrier is at least as strong as the crash-
 475 tested barrier [6]. The AASHTO Bridge Specification
 476 provides a Load and Resistance Factor Design (LRFD)
 477 procedure for designing traffic railings [4]. Resistance
 478 factors for various barrier components can be found in
 479 Table 3.4.1-1 in the AASHTO LRFD Bridge Specification
 480 [4]. The resistance factor for vehicle collision events (CT)
 481 in the extreme event II category is given as 1.0. Table
 482 A13.2-1 provides three specific design loadings that must

be used in analyzing a barrier for Report 350 test level 3 483
 and 4 as required by AASHTO LRFD Table A13.2-1. 484
 These are summarized in Table 3. 485

In principle for a system like the aluminum bridge railing 486
 with posts and beam elements there are six load cases 487
 required by the AASHTO LRFD specification for each 488
 test level: 489

- Transverse loads 490
 - Centered on the post and 491
 - Centered on the mid-span. 492
- Longitudinal loads 493
 - Centered on the post and 494
 - Centered on the mid-span. 495
- Vertical loads 496
 - Centered on the post and 497
 - Centered on the mid-span. 498

Performing the analyses for the aluminum bridge railing 499
 would, therefore, involve 12 separate analyses. Fortunately, 500
 many of these analyses are not really necessary and can be 501
 eliminated. For example, if a barrier passes the test level 502
 four analyses there is no point in performing the test level 503
 three analyses since the test level three loading is a lower 504
 intensity distributed load applied at a lower height. This 505
 reduces the total number of tests to six. 506

Both transverse loading tests for test level four are 507

Table 2 Results of simulation of Report 350 Test 3-11 conditions for a rigid F-shape barrier

Test parameter	Simulation
<i>Test vehicle</i>	
Type	C2500
Test inertial mass	2008 kg
<i>Impact conditions</i>	
Velocity	100.0 km/h
Angle	25.0 deg
<i>Exit conditions</i>	
Velocity	78 km/hr
Angle	5.8 deg
<i>Occupant impact velocity (OIV)</i>	
Longitudinal	6.8 m/s
Lateral	9.1 m/s
<i>Occupant ridedown acceleration (ORA)</i>	
Longitudinal	5.6 g's
Lateral	8.4 g's
<i>CEN parameters</i>	
THIV	39.7 km/hr
PHD	10.4 g's
ASI	2.1
<i>Max. 50 msec average</i>	
Longitudinal	11.6 g's
Lateral	16.6 g's
<i>Vehicle rotations</i>	
Maximum Roll	13.0 deg
Maximum Pitch	4.1 deg
Maximum Yaw	31.1 deg

508 necessary since the transverse load may fail the post or its
 509 connection to the deck (i.e., the loading centered on the
 510 post) or the truss-core panels in bending (i.e., the loading
 511 centered on the midspan). These two tests are probably
 512 the two most important tests in the group. The longitudinal
 513 load arises primarily from vehicle-barrier friction and
 514 potential vehicle-barrier snagging. The aluminum bridge
 515 railing has a smooth face so snagging between the vehicle
 516 and barrier is very unlikely and friction between the barrier

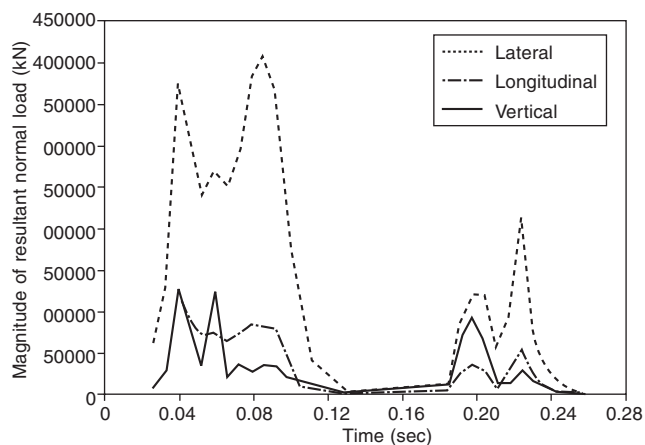


Figure 10 Lateral, longitudinal and vertical contact force resultants as a function of time for a Test 3-11 impact with a rigid F-shaped barrier.

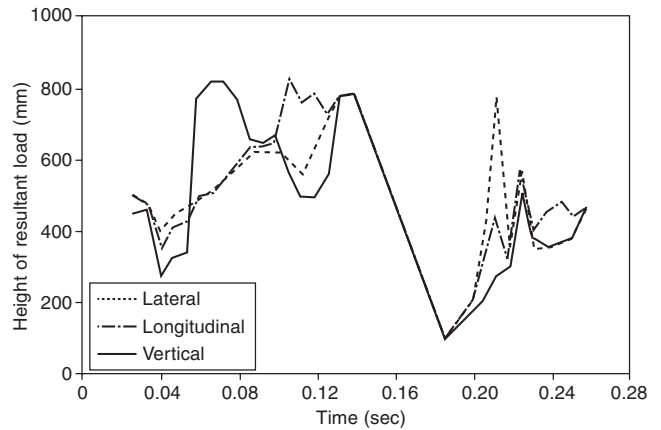


Figure 11 Lateral, longitudinal and vertical height of force resultant as a function of time for a Test 3-11 impact with a rigid F-shaped barrier.

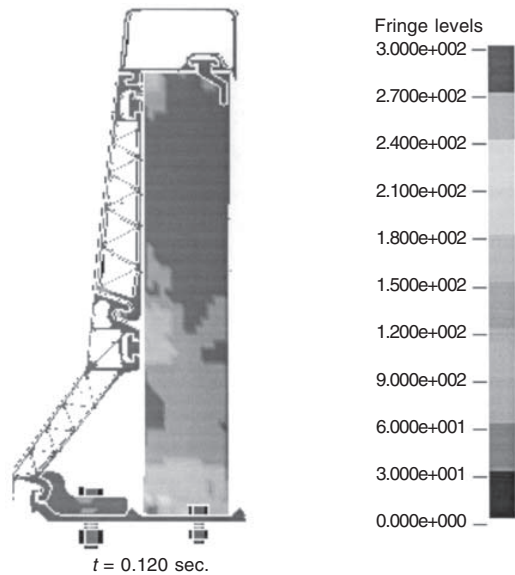


Figure 12 Von Mises stress contours of the aluminum bridge parapet under Report 350 Test 3-11 conditions.

components is small since it involves metal to metal contact. 517
 An analysis of the longitudinal loads is therefore not needed. 518
 The vertical loads represent the cargo deck of a truck 519
 striking the top of the barrier. Barriers like the aluminum 520
 bridge parapet and median barrier that include short posts 521
 will be very strong if struck from above directly on the 522
 post. The vertical load centered on the midspan is a more 523
 revealing test of the barrier since the top rail and truss 524
 core panels need to transfer the load in bending to the 525
 posts and deck. The adequacy of the aluminum bridge 526
 railing design can, therefore, be assessed by evaluating 527
 the following three load cases: 528

- A transverse load centered on the post, 529
- A transverse load centered on the mid-span, and 530
- A vertical load centered on the mid-span. 531

The AASHTO LRFD Bridge Specification provides 532
 analysis procedures for simple barrier types like concrete 533

534 parapet railings and post-and-beam type railings.
 535 Unfortunately, the aluminum parapet bridge railing is a
 536 complex structure that involves complicated geometry and
 537 extruded truss-core panels that do not lend themselves to
 538 simple hand analysis methods. The aluminum bridge railing
 539 is highly indeterminate (this is beneficial since it provides
 540 more load paths but it makes the analysis more complicated)
 541 so a non-linear quasi-static finite element analysis using
 542 the loads required by the AASHTO LRFD Bridge
 543 Specification is the only possible method for assessing
 544 the adequacy of these two railings by the AASHTO LRFD
 545 procedure. The results of the quasi-static analyses for test
 546 level four are presented in the following section. The
 547 analyses were performed using LS-DYNA where the loads
 548 shown in Table 3 were applied quasi-statically to the same
 549 barrier models discussed earlier in the report.

Table 3 Equivalent Static Loads for Test Levels 3 and 4 based on the AASHTO LRFD Bridge Specification

Property	Transverse	Longitudinal	Vertical
<i>Test Level 3</i>			
Load (kN)	240	80	20
Length (mm)	1220	1220	5500
Distributed load (kN/m)	200	65	5
Height of application (mm)	685	685	top
<i>Test Level 4</i>			
Load (kN)	240	80	80
Length (mm)	1070	1070	5500
Distributed load (kN/m)	225	75	15
Height of application (mm)	810	810	top

550 Application of quasi-static loads to the F-shape parapet 551 bridge railing

552 240 kN transverse load centered on a middle post

553 The first load case involves a 240 kN load applied vertically
 554 across the face of the top rail at a height of 810 mm above
 555 the bridge deck. The load was applied centered on a middle
 556 post and extended longitudinally 535 on each side of the
 557 post. This loading provides a critical test of the strength
 558 of the post, baseplate and front bolts. Figure 13 shows a
 559 cross-section view through the post at the point of
 560 maximum deflection. The maximum deflection at the
 561 height of load application (i.e., 810 mm) was 48 mm. The
 562 maximum stresses in the post, as shown in Figure 26,
 563 were located on the tension side of the web above the
 564 point where the upper and lower truss core panels are
 565 connected. The maximum post stress was 317 MPa, close
 566 to the failure stress of the material. While the stresses
 567 were approaching high levels, the deflection was still quite
 568 moderate, the deformations were very localized and the
 569 barrier system still maintained its integrity. The tongue-
 570 and-groove connections between the lower and upper truss
 571 core panels and the upper truss core panel and the top

572 rail all maintained their integrity and did not pull open.
 573 The stresses in these connections generally remained less
 574 than the yield stress of the 6063-T6 aluminum material.
 575 There were several very small regions of near-failure stress
 576 due to contact stresses in the connection between the
 577 upper and lower truss core panels but these represent
 578 very localized stresses. The base plate experienced high
 579 bending stresses on a section through the bolt hole as
 580 shown in Figure 13. The maximum stress in the base
 581 plate was 275 MPa, high but only slightly above the 241
 582 MPa yield stress of the material and still well below the
 583 317 MPa failure stress of the material. The net tensile
 584 force on each of the 24-mm diameter front bolts was 290
 585 kN, just below the 293 kN minimum tensile strength of
 586 an M24 A325 bolt. The results of this quasi-static analysis
 587 of the AASHTO LRFD transverse loading for test level
 588 four indicate that the bridge railing has sufficient strength
 589 to successfully redirect the 8000S truck in a Report 350
 590 TL-4 impact.

240 kN transverse load centered on the midspan

591 The second load case involves a 240 kN load applied
 592 vertically across the face of the top rail at a height of 810
 593 mm above the bridge deck. The load was applied centered
 594 on the midspan point between two middle posts and
 595 extended longitudinally 535 on each side of the mid-span
 596 point. This loading provides a critical test of the strength
 597 of the upper and lower truss core panels and the top rail.
 598 Figure 14 shows a cross-section view through the post at
 599 the point of maximum deflection. The maximum values
 600 of the effective stress contours in Figure 14 are set to the
 601 failure stress of the aluminum material, 317 MPa. There
 602 were two points of high stress concentration in the posts
 603 as shown in Figure 30: one at the base of the web at the
 604 front of the post and the other in the flange just above the
 605 connection point of the front panel to the post at
 606 approximately 310 mm above the base. These post stresses
 607 were high but below the failure stress of 317 MPa. The
 608 maximum effective stress in the upper toe clip of the
 609 bolted base plate was less than 140 MPa at the post location.
 610 There were some higher stress concentrations at the mid-
 611 span toe clip locations but aside from these local
 612 concentrations the stresses were also generally below 140
 613 MPa at the midspan toe clip as well. The maximum
 614 deflection at the height of load application (i.e., 810 mm)
 615 was 42 mm and this occurred at the mid-span. The
 616 maximum stress in the truss core panels was approximately
 617 255 MPa, just slightly above the yield stress. The stresses
 618 are relatively low in the truss core panels because of the
 619 way they are attached to the rest of the system and the
 620 point of loading. The load is applied to the top rail, but
 621 the connection of the top rail to the truss core panels is
 622 not much more than friction at any point between posts.
 623 When load is applied to the top rail, the top rail has to
 624 transfer the load to the post and then the post transfers
 625 the load back to the truss core panels through the bolted
 626 connections. The net tensile force on each of the 24 mm
 627 diameter front bolts was 171 kN, well under the 293 kN
 628

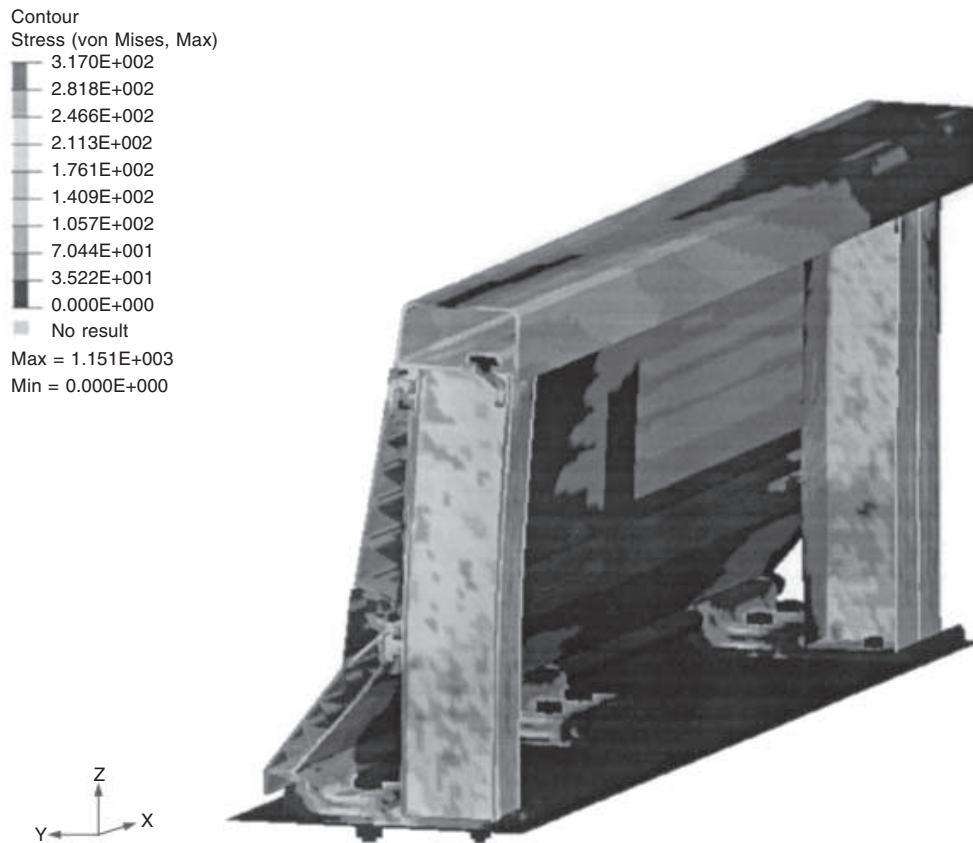


Figure 13 Effective stress contour and section cut at the point of maximum deflection for the AASHTO LRFD transverse centered-on-post test level four load case.

629 minimum tensile strength of an M24 A325 bolt. The results
630 of this quasi-static analysis of the AASHTO LRFD
631 transverse loading for test level four indicate that the bridge
632 railing has sufficient strength to successfully redirect the
633 8000S truck in a Report 350 TL-4 impact.

634 **80 kN vertical load centered on midspan**

635 The third load case involves an 80 kN vertical load applied
636 across the top face of the top rail. The load was applied
637 centered on the mid-span point to maximize the chance
638 of bending the top rail and truss-core panels. The load
639 extends 2775 mm on each side of the mid-span point.
640 This loading provides a critical test of the bending strength
641 of the top rail if the cargo deck of a truck should strike
642 the top of the barrier. The maximum vertical deflection
643 of the top rail at the point of load application (i.e., the
644 mid-span) was 13.4 mm. Figure 15 shows the effective
645 stress along the top rail, the maximum value being just
646 over the yield stress. The stresses in the post are quite low
647 with the exception of the area at the bottom front of the
648 flange where they slightly exceed the yield stress. The top
649 rail does experience some minor localized deformations
650 but in general the stress, strains and deformations are
651 very low throughout the barrier system under this loading
652 condition. The results of this quasi-static analysis of the
653 AASHTO LRFD vertical loading for test level four
654 indicates that the bridge railing has sufficient strength to
655 successfully sustain a vertical impact with the cargo deck

of an 8000S truck in a Report 350 TL-4 impact. 656

The foregoing quasi-static analyses show that the 657
aluminum F-shape parapet bridge railing has sufficient 658
strength to meet the requirements of the AASHTO LRFD 659
Specification for TL-4 conditions. 660

661 **CONCLUSIONS**

The foregoing analyses have demonstrated by the use of 662
the non-linear dynamic finite element program LSDYNA 663
that the aluminum parapet bridge railing can withstand 664
the Test 3-11 pickup truck loading and only sustain minor 665
deformations. The integrity of the barrier was maintained 666
throughout the loading and only minor localized permanent 667
deflections resulted. Most of the material in the barrier 668
behaved elastically indicating that there was considerable 669
reserve capacity. The aluminum parapet bridge railing 670
can be considered essentially rigid F-shape barriers and 671
since rigid F-shape barriers are widely considered to satisfy 672
Report 350 test level three, these barriers should be 673
considered test level three barriers as well. 674

The AASHTO LRFD procedure was also followed to 675
evaluate the aluminum bridge parapet for test level four 676
conditions. The quasi-static analyses showed that the barrier 677
contains sufficient strength to resist the loads that would 678
be expected in a test level four impact. In all cases, the 679
barrier deformations, material stress and other structural 680

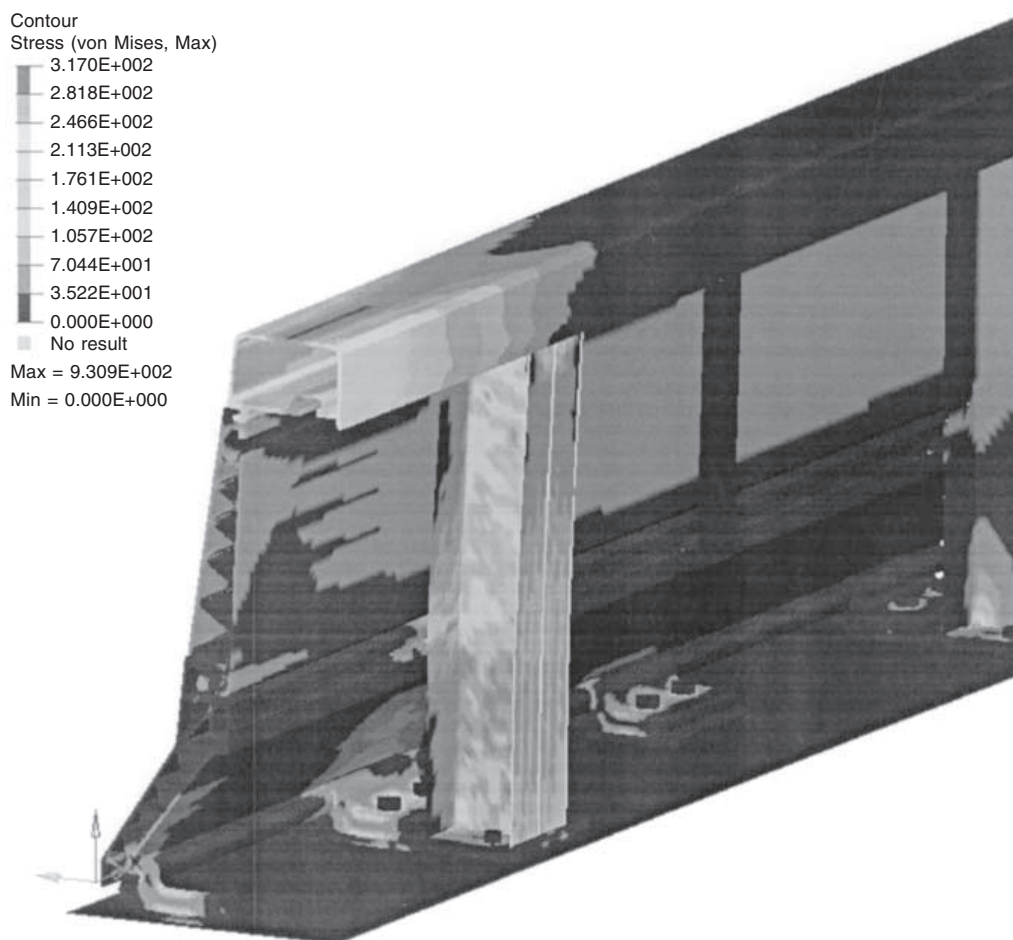


Figure 14 Effective stress contours on the upper section of the barrier at the point of maximum deflection for the AASHTO LRFD transverse centered-on-post test level four load case.

681 performance parameters were acceptable and, in fact,
682 showed that the barrier has considerable reserve capacity
683 even in test level four conditions.

684 For both the dynamic test level three analysis and the
685 quasi-static AASHTO LRFD test level four analysis, the
686 barrier remained intact, experiencing only minor
687 deformations and reasonable local deformations. The
688 barrier performed essentially rigidly since in all cases the
689 dynamic deflections are under 50 mm, usually significantly
690 less. Since the barrier behaved rigidly, it is reasonable to
691 expect that it will perform much like other crash-tested
692 essentially rigid F-shape barriers. Crash tests with the
693 aluminum bridge parapet railing are very likely to result
694 in acceptable performance in both test levels three and
695 four conditions.

696 REFERENCES

- 697 1. BUTH, C E, HIRSCH T J and McDEVITT, C F. "Performance
698 Level 2 Bridge Railings," Transportation Research Record
699 1258, Transportation Research Board, Washington, D.C.,
700 1990
- 701 2. BRONSTAD, M E, CALCOTE, L R and KIMBALL, C E. Concrete
702 Median Barrier Research, Report FHWA-RD-77-4, Federal
703 Highway Administration, Washington, D.C., 1976.

3. ROSS, H E, SICKING, JR, D L ZIMMER, R A and MICHIE, J D 704
"Recommended Procedures for the Safety Performance 705
Evaluation of Highway Features," Report 350, National 706
Cooperative Highway Research Program, Washington, D.C., 707
1993. 708
4. Aashto, "Aashto LRFD Bridge Design Specifications," SI 709
Units, 2nd ed with interim specifications through 2000, 710
American Association of State Highway and Transportation 711
Officials, Washington, D.C., 1998 712
5. WRIGHT, F G. "Bridge Rail Analysis," FHWA Memorandum, 713
Federal Highway Administration, Washington, D.C., 16 May 714
2000. 715
6. BUTH, C E. *et al.* "Safer Bridge Railings," Vol. I, FHWA 716
Technical Report No. FHWA-RD-82-072, Federal Highway 717
Administration, Washington, D.C., June 1984. 718
7. TISO, P, PLAXICO, C A and RAY, M H. "An Improved Truck 719
Model for Roadside Safety Simulations: Part II – Suspension 720
Modeling," Transportation Research Record No. 1797, 721
Transportation Research Board, Washington, D.C., 2002 722
8. ORENGO, F, PLAXICO, C A and RAY, M H. "Modeling Tire 723
Blow-out in Roadside Hardware Simulations Using LS- 724
DYNA," *Proceedings of the Annual Meeting*, American Society 725
of Mechanical Engineers, Reston, VA, 2003. 726
9. OLDANI, E. *Study of a New Aluminum Bridge Railing Design 727
for Suspended Bridges*, Thesis, Department of Aerospace 728
Engineering, Politecnico di Milano, Milan, Italy, November 729
2003. 730

